

Aeroelastic instability of long-span bridges: contributions to the analysis in frequency and time domains

Vincenzo Sepe[†]

*Dipartimento di Ingegneria Strutturale e Geotecnica - Università di Roma "La Sapienza" -
via Eudossiana 18 - 00184 Roma, Italy*

Luca Caracoglia[‡]

Dipartimento di Ingegneria Civile - Università di Trieste - p.le Europa 1 - 34127 Trieste, Italy

Piero D'Asdia^{†‡}

*Dipartimento di Scienze, Storia dell' Architettura e Restauro - Università di Chieti "G. D' Annunzio" -
Viale Pindaro 42 - 65127 Pescara, Italy*

Abstract. According to research currently developed by several authors (including the present ones) a multimode approach to the aeroelastic instability can be appropriate for suspension bridges with very long span and so with close natural frequencies. Extending that research, this paper deals in particular with: i) the role of along-wind modes, underlined also by means of the *flutter mode* representation; ii) the effects of a variation of the mean wind speed along the span. A characterisation of the response in the time domain by means of an energetic approach is also discussed.

Key words: aeroelastic instability; long-span suspension bridges; frequency-domain multimode analysis; time-domain energetic approach.

1. Introduction

In the evaluation of the effects of wind on long span suspended bridges, it is quite usual nowadays - along with wind tunnel tests on in scale models - to perform numerical simulations, carried out by means of either very complex or very simplified mechanical models. Due to the large number of degrees of freedom involved, the former, e.g., non-linear finite elements models (FEM), often tend to obscure the essential points of the response and therefore are not convenient at a preliminary design stage; on the contrary, simplified models can give more straightforward information in most cases. Such a simple and well known model is the two-degrees-of-freedom (2dof) sectional model, that

[†] Assistant Professor

[‡] Ph. D. Student

^{†‡} Professor

can often give a satisfactory estimation of the critical wind speed for the aeroelastic instability.

In the recent scientific literature, the opportunity is widely discussed of using a multimode approach to the aeroelastic instability, that takes into account several natural modes of the system around a reference equilibrium configuration, instead of the first pair of modes (vertical and torsional) of the sectional model. In particular, previous papers of the authors (Sepe, Ciappi and D'Asdia 1996, D'Asdia and Sepe 1998) underline the opportunity of the multimode approach for very long span bridges characterised by high modal density.

Extending that papers, the research reported here deals in particular with the following aspects:

- a) influence of the lateral modes on the critical conditions of aeroelastic instability; as recently underlined (D'Asdia and Sepe 1998, Katsuchi 1997) this aspect can become very important, depending on the deck shape; in this paper, the role of lateral modes is underlined through the representation of the *flutter mode*, that is obtained by means of an eigenvalue - eigenvector procedure implemented *ad hoc* starting from natural modes given by a FEM nonlinear analysis programme;
- b) effect of the variation along the axis of the time average of wind speed, e.g., due to different topographical conditions, that can become relevant for an increasing length; possible implications of such circumstance are dealt with by means of the multimode approach;
- c) the convenience is also discussed of integral measures for representing the system response in the time domain, given by a FEM model with a huge number of degrees of freedom and therefore sometimes difficult to understand. An immediate representation of the response is shown through the *total energy* of the system or through the *input energy*, corresponding to the work done by forces due to fluid-structure interaction. It is well known that the character of this wind-structure energy exchange is modified near to critical conditions of aeroelastic instability, due to synchronisation mechanism between modes that extracts systematically energy from the fluid.

2. Multimode approach

The simplest and well known way to deal with the aeroelastic stability of a bridge is to consider a rigid section model, that takes into account only displacements due to the first vertical and torsional modes (2dof).

Namely, a *computational section model* can be defined by introducing modal characteristics of the bridge (e.g., known through a FEM analysis) and aerodynamic data of the deck; for wind tunnel tests it is also widely used an *experimental section model*, that consists of an in-scale model of the deck preserving its most aerodynamically relevant geometrical features, and elastically constrained in such a way to reproduce the vertical and torsional modal frequencies of the bridge (with an appropriate scale factor).

It is worth to stress that the correspondence between the 2dof rigid section model and the effective behaviour of the system requires a perfect similarity of the two modes involved. If this hypothesis is not completely verified but the difference between vertical and torsional modal shapes is not very large, the aerodynamic coupling can still occur, but in this case appropriate corrective coefficients should be introduced in the computational section-model.

The contribution of an increasing number of natural modes becomes more and more important with an increasing length of the bridge, and in particular lateral displacements can play a significant role (D'Asdia and Sepe 1998). Nevertheless, a multimode approach to the aeroelastic instability,

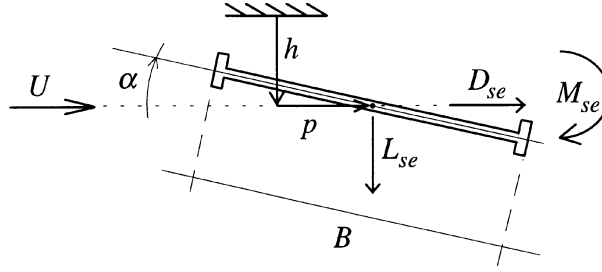


Fig. 1 Coordinates and aeroelastic actions on the deck

described since 70's (Scanlan and Tomko 1971, Scanlan 1978), has only recently been used in technical applications (Tanaka, Yamamura and Tatsumi 1992, Jain, Jones and Scanlan 1996, Katsuchi, Jones, Scanlan and Akiyama 1997, D'Asdia and Sepe 1998). It extends the 2dof model and consists in describing self-excited oscillations around a significant equilibrium configuration through linearised equations, taking into account an adequate number of natural modes. In the approach described in D'Asdia and Sepe (1998) and summarised here, the natural modes are obtained by a FEM analysis taking into account geometrical non-linearities and stiffnesses, and the critical wind speed is found by means of an eigenvalue - eigenvector procedure implemented *ad hoc*.

Denoted by x the coordinate along the axis, by $h(x, t)$ and $p(x, t)$ the non-dimensional vertical and transversal (*along-wind*) displacements (displacements scaled with the width of the deck B) and by $\alpha(x, t)$ the torsional rotation (Fig. 1), by $h_j(x)$, $p_j(x)$, $\alpha_j(x)$ the corresponding displacement components of the j -th natural mode shape and by ξ_j the j -th modal coordinate, the displacement response is described by

$$h(x, t) = \sum_j \xi_j(t) h_j(x); \quad p(x, t) = \sum_j \xi_j(t) p_j(x); \quad \alpha(x, t) = \sum_j \xi_j(t) \alpha_j(x) \quad (1)$$

Denoting by (\cdot) the derivative with respect to the time t , by I_j , ζ_j , and ω_j the j -th modal inertia, structural damping and angular frequency, respectively, and taking into account the first N modes, the dynamics is described by the equations

$$I_j [\ddot{\xi}_j + 2\zeta_j \omega_j \dot{\xi}_j + \omega_j^2 \xi_j] = Q_j)_{se} ; \quad j = 1, 2, \dots, N. \quad (2)$$

In Eq. (2) $Q_j)_{se}$ are generalised self-excited forcing terms that depend on the contributions of the whole set of natural modes. The lift and drag forces and the aeroelastic moment per unit length L_{se} , D_{se} , M_{se} (Fig. 1) can be expressed in the classical Scanlan formulation (Scanlan and Tomko 1971, Scanlan 1978, Scanlan 1987, Simiu and Scanlan 1996) as a function of coordinates h , p and α and corresponding velocities \dot{h} , \dot{p} and $\dot{\alpha}$ through coefficients H_j^* , P_j^* and A_j^* known as *flutter derivatives*:

$$\begin{aligned} L_{se}(\dot{h}, \dot{\alpha}, \alpha) &= \frac{1}{2} \rho U^2 B \left[KH_1^*(K) \frac{\dot{h}}{U} + KH_2^*(K) \frac{B \dot{\alpha}}{U} + K^2 H_3^*(K) \alpha \right] \\ D_{se}(\dot{p}, \dot{\alpha}, \alpha) &= \frac{1}{2} \rho U^2 B \left[KP_1^*(K) \frac{\dot{p}}{U} + KP_2^*(K) \frac{B \dot{\alpha}}{U} + K^2 P_3^*(K) \alpha \right] \\ M_{se}(\dot{h}, \dot{\alpha}, \alpha) &= \frac{1}{2} \rho U^2 B^2 \left[KA_1^*(K) \frac{\dot{h}}{U} + KA_2^*(K) \frac{B \dot{\alpha}}{U} + K^2 A_3^*(K) \alpha \right] \end{aligned} \quad (3)$$

Here, ρ , B and U denote air density, deck width and mean wind speed, respectively, the latter assumed as horizontal and orthogonal to the bridge axis. Eq. (3) corresponds to the “basic” representation of aeroelastic forces; the contributions of “added-mass” terms related to the accelerations, included by some authors (e.g., Katsuchi, Jones, Scanlan and Akiyama 1997), are expected to play a negligible role for the example under consideration, and have therefore been omitted.

Flutter derivatives H_j^* , P_j^* and A_j^* can be obtained by experiments in wind tunnel and expressed as a function of the *reduced frequency* $K = B\omega / U$, where ω denotes the angular frequency of the imposed motion.

It results

$$Q_j)_{se} = \int_{span} [L_{se}h_j(x)B + D_{se}p_j(x)B + M_{se}\alpha_j(x)]dx \quad (4)$$

Defining as *critical* the wind speed corresponding to harmonic oscillations (that is, not decreasing nor diverging for given initial conditions), the equations governing the motion can be expressed in the frequency domain assuming the following notations

$$\xi = [\xi_1, \dots, \xi_N]^T = \xi_0 e^{i\omega t} = \xi_0 e^{iKs}, \quad \xi \in \mathbb{C}^N, \quad \xi_0 \in \mathbb{C}^N, \quad \omega \in \mathbb{R}, \quad s = \frac{Ut}{B} \quad (5)$$

where $i^2 = -1$, ξ_j are complex amplitudes containing also information on the phase-lag between motion components and \mathbb{C}^N , \mathbb{R} denote complex and real spaces.

In matrix form, the equations of motion turn out

$$[C(K, \omega) + iD(K, \omega)]\xi_0 = 0 \quad (6)$$

where the coefficients C_{ij} , D_{ij} of the respective $N \times N$ matrices are reported in Appendix.

The existence of steady-state oscillations with amplitude ξ_0 is only possible if both the real and imaginary part of the determinant $\det(C + iD)$ vanish, that leads to equations in K and ω , whose solution can be sought numerically. Finally, the critical (or *flutter*) speed $U_C = B\omega_C / K_C$ comes out, where ω_C denotes the angular frequency of the critical oscillating configuration (*flutter mode*), to which several natural modes contribute, possibly out of phase but synchronised to each other due to aerodynamic forces; the critical shape ξ_{0c} corresponds to the eigenvector of the problem

$$[C(K_C, \omega_C) + iD(K_C, \omega_C)]\xi_{0c} = 0 \quad (7)$$

As underlined for the 2dof rigid section model, the similarity between modal shapes (e.g., b , c , d in Fig. 3) is a necessary condition for the aerodynamic coupling; if there is an appropriate phase-lag between motion components, coupling can also raise even if the aerodynamic damping is positive in each mode.

3. Example: The proposed bridge on the Messina Strait

The multimode approach described in previous section has been applied to the current design of the proposed bridge on the Messina Strait, with main span of 3300 m (Fig. 2).

The first 20 natural modes around the equilibrium configuration in average (*static*) wind flow have been evaluated through a FEM model (5000 dof) and a computer code able to take into account geometrical non-linearities and stiffnesses (relevant modes in Fig. 3). Aeroelastic derivatives in Fig.

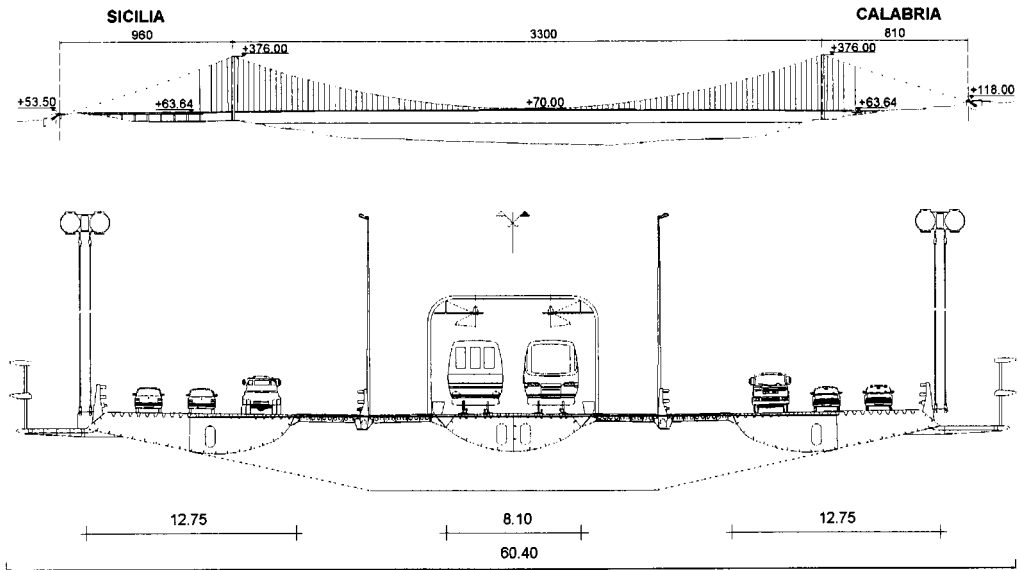


Fig. 2 Current design of the proposed bridge on the Messina Strait (measures expressed in meters)

mode	angular frequency ω_j (rad/s)	period T_j (s)	main component
<i>a</i>	0.195	32.2	1st lateral
<i>b</i>	0.352	17.8	2nd lateral
<i>c</i>	0.380	16.5	1st vertical
<i>d</i>	0.500	12.6	1st torsional
<i>e</i>	0.501	12.5	3rd lateral
<i>f</i>	0.508	12.4	2nd vertical
<i>g</i>	0.606	10.4	2nd torsional
<i>h</i>	0.626	10.0	4th lateral
<i>i</i>	0.677	9.3	3rd vertical
<i>l</i>	0.705	8.9	5th lateral
<i>m</i>	0.803	7.8	3rd torsional

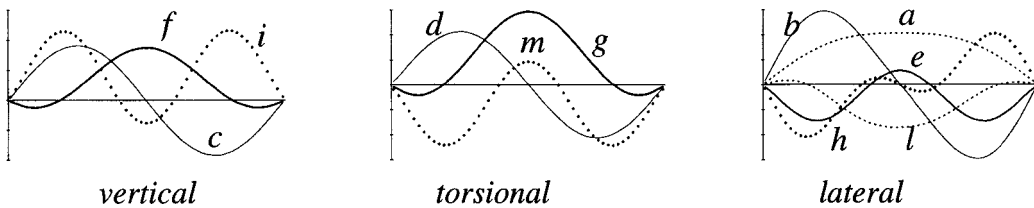


Fig. 3 Natural modes around the dead loads equilibrium configuration

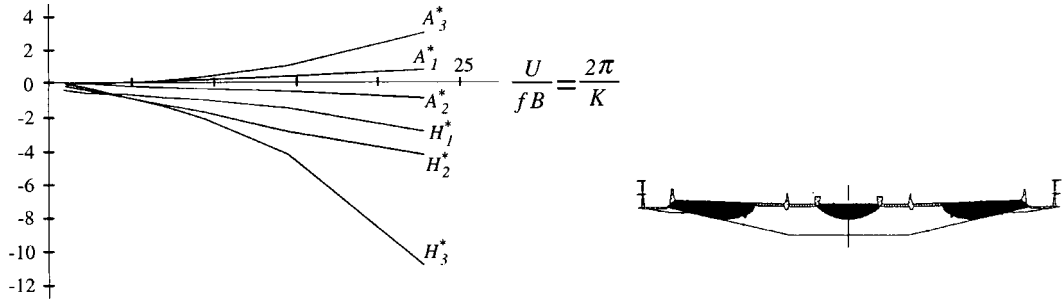


Fig. 4 Flutter derivatives of the Messina Bridge. Data from design reports and from Zasso (1996) ($f = \omega / (2\pi)$)

4 and average values of mass M per unit length and torsional mass moment of inertia I per unit length ($M = 5.5 \cdot 10^4$ kg/m, $I = 2.8 \cdot 10^7$ kg \cdot m²/m) have been used, and a structural damping ζ_j varying from 0.6% to 0.8% has been assumed, depending on the mode.

With these values the multimode approach gives (D'Asdia and Sepe 1998) the critical values $U_C = 94$ m/s, $K_C = 0.276$, $\omega_C = 0.418$. In the example under consideration, the solution obtained through the multimode approach including several vertical, lateral and torsional modes is almost coincident with the solution given by the 2dof rigid section model, probably as a consequence of the excellent aerodynamic behaviour of the proposed three-box deck, and is also in good agreement with wind tunnel tests on rigid section model and full bridge aeroelastic model. However, different bridge geometry could amplify such differences, or even show phenomena not forecast by the rigid section model. The role of lateral modes is underlined in recent papers (Katsuchi 1997, Katsuchi, Jones, Scanlan and Akiyama 1997) on the Akashi-Kaikyo bridge, opened in 1998, with the 1990 meters main span the longest so far built; in such a case, in fact, the multimode analysis gives an unacceptable overestimation of the flutter speed (more of 135 m/s instead of 75 m/s) if it is performed neglecting the cross aeroelastic derivatives corresponding to the drag, i.e., those associated to the torsional mode (P_2^* , P_3^* in Eq. 3) and to the vertical mode, according to the extended formulation introduced in (Katsuchi, Jones, Scanlan and Akiyama 1997).

In any case, the multimode approach should not be *a priori* excluded whenever aerodynamic coupling between modes is expected to arise due to closeness of natural frequencies, as it is likely to occur for so deformable systems.

The critical eigenvector ξ_{0C} of Eq. (7), normalised to unitary modulus, is reported in Table 1. The contributions of the first three modes are represented graphically in Fig. 5; it can be observed that the amplitudes h and p of vertical and lateral modes, representing the ratios between corresponding displacements and the deck width B (cf. Sec. 2), are comparable also in quantitative terms with the amplitude of torsional mode. It is worth to remember that the aerodynamic coupling leading to flutter requires a phase-lag between the components of motion, so that the work done by aeroelastic forces turns out to be, in the average, larger than the energy dissipated by mechanical damping.

As expected, the prominent role of modes c and d is evident from Table 1 and Fig. 5, while the contribution of higher modes is negligible. It can also be observed that the only significant contribution of lateral modes is given by the skew-symmetric mode b , approximately one tenth of the vertical mode c contribution; moreover, the lateral mode is only relevant to the flutter mode shape, while the flutter speed is only modified of a few meters per second.

Two different representations in time-history of the flutter mode for the Bridge on the Messina

Table 1 Eigenvector ξ_{0c} corresponding to the flutter mode for the current design of the Messina Bridge

Mode	Re(ξ_{0c})	Im(ξ_{0c})	Modulus	Phase [°]	main component
<i>a</i>	0.00060	0.00013	0.00061	12.5	1st Lateral
<i>b</i>	-0.08085	0.06067	0.10108	143.2	2nd Lateral
<i>c</i>	0.91437	0.00000	0.91437	0.0	1st Vertical
<i>d</i>	0.19645	-0.33917	0.39195	-59.9	1st Torsional
<i>f</i>	0.00104	0.00481	0.00493	77.8	2nd Vertical
<i>g</i>	-0.00699	-0.00004	0.00699	180.3	2nd Torsional
<i>i</i>	-0.00052	0.00054	0.00075	134.1	3rd Vertical
<i>m</i>	-0.00005	0.00076	0.00077	93.5	3rd Torsional

(*Re*, *Im*: real and imaginary parts)

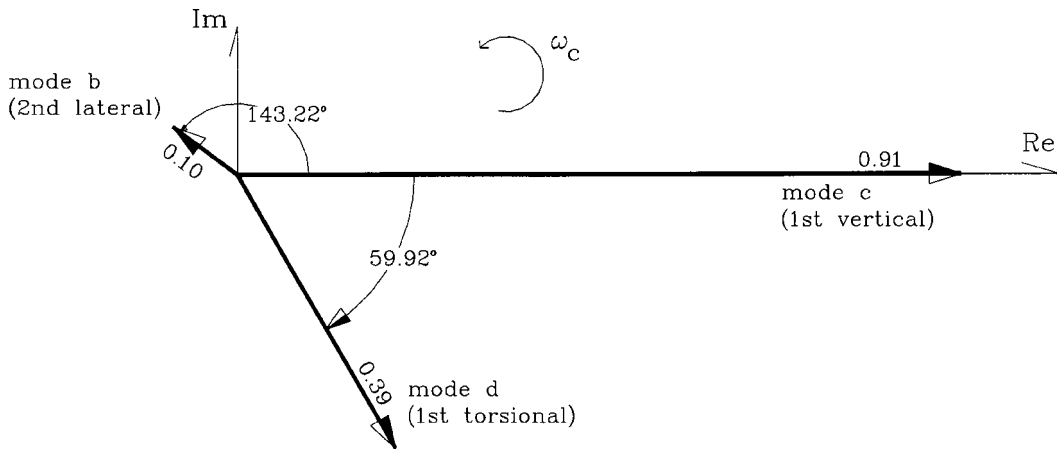


Fig. 5 Polar representation of the most significant contributions to the flutter mode for the current design of the Messina Bridge

Strait are reported in Fig. 6 and Fig. 7, where subsequent configurations are separated by time intervals of duration $T_c/8$, T_c being the period of the critical oscillation (approximately equal to 15 seconds). In Fig. 6 drag force, lift force and aerodynamic moment are also represented, according to Eq. (3).

Fig. 7 confirms that the main contributions to flutter mode are given by the skew-symmetric modes *b*(lateral), *c*(vertical), *d*(torsional). However, due to the higher modes, the time history of displacement *h* and rotation *a* are not perfectly similar, although this cannot be appreciated due to the scale factor of the representation.

3.1. A different example

In the previous section it was shown that a truss-type deck (as for the Akashi-Kaykio Bridge), very stiff and with relatively bad aerodynamic performances, requires the multimode technique as the only way to get a correct flutter speed; in fact, either the 2dof section-model or a simplified multimode approach performed by neglecting some terms of aerodynamic coupling, turned out to be insufficient.

$\Omega_{m_c} = 0.4179 \text{ rad/s}$ - $T_c = 15.04 \text{ s}$ - $U_c = 94 \text{ m/s}$
 Section n.29 [1/4 span]

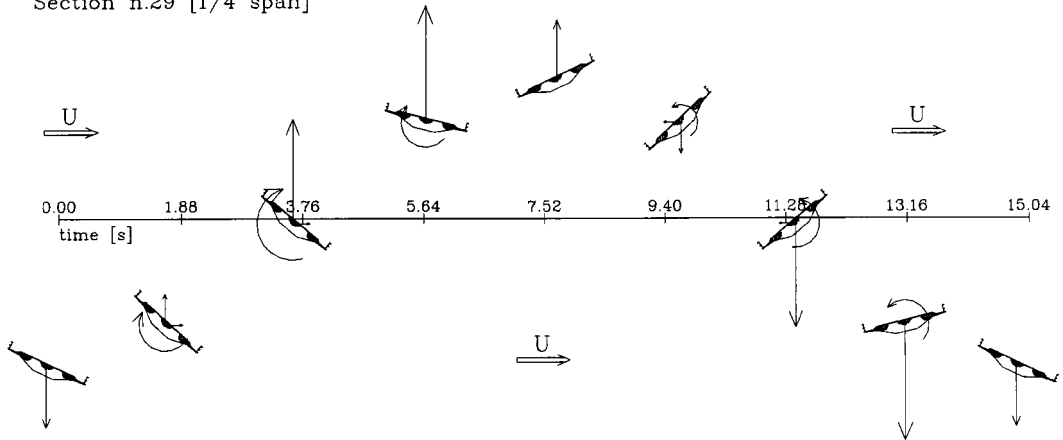


Fig. 6 *Flutter mode* for the current design of the Messina Bridge (motion of a quarter-span section, subsequent configurations separated by a time interval $T_C/8$, where $T_C = 2\pi/\omega_C$); aeroelastic lift, drag and moment, according to Eq. (3), are also shown

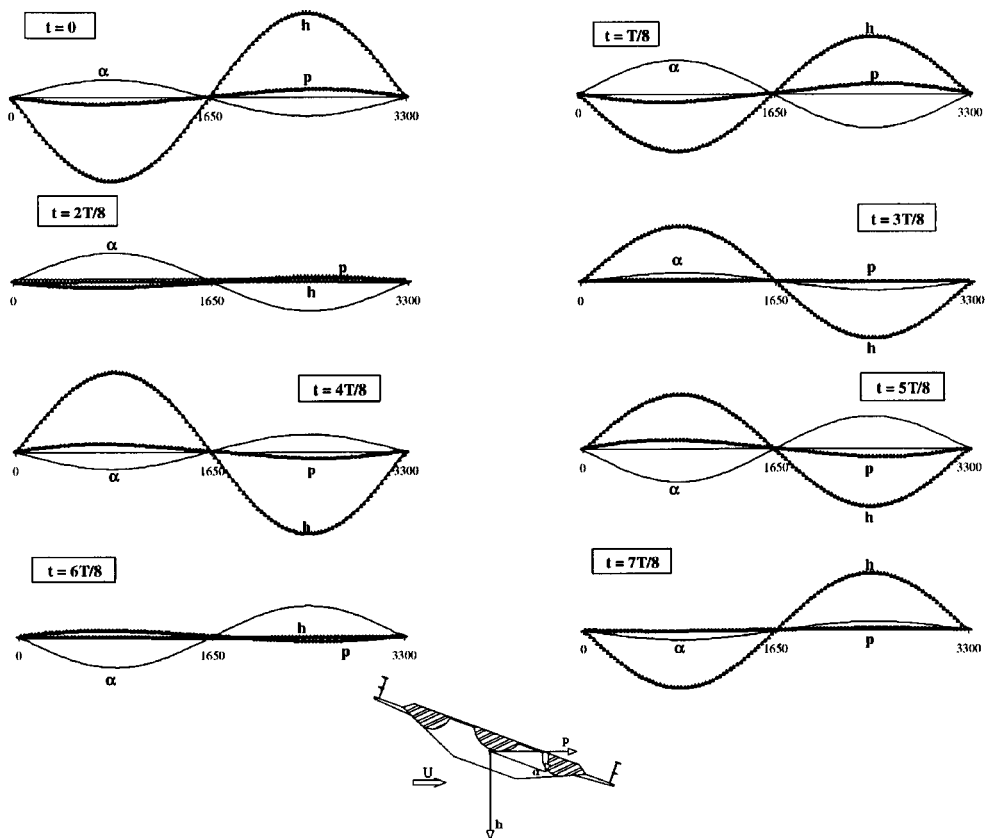


Fig. 7 *Flutter mode* for the current design of the Messina Bridge (motion of the axis in the central span, subsequent configurations separated by a time interval $T_C/8$, where $T_C = 2\pi/\omega_C$)

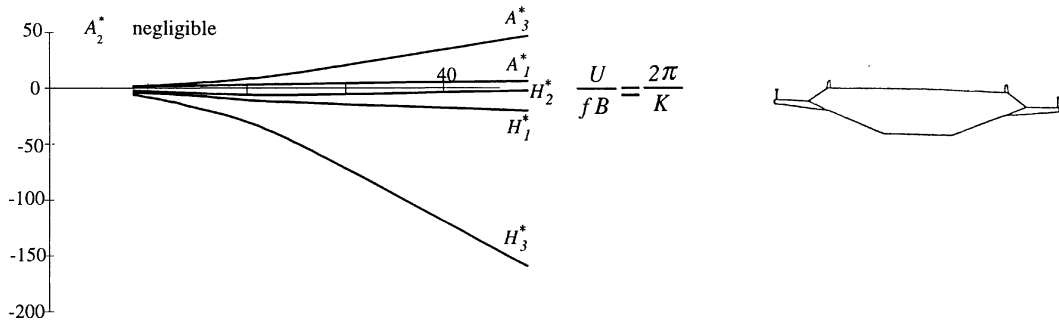


Fig. 8 Flutter derivatives of the Humber Bridge. Data from Zasso (1996) ($f = \omega / (2\pi)$)

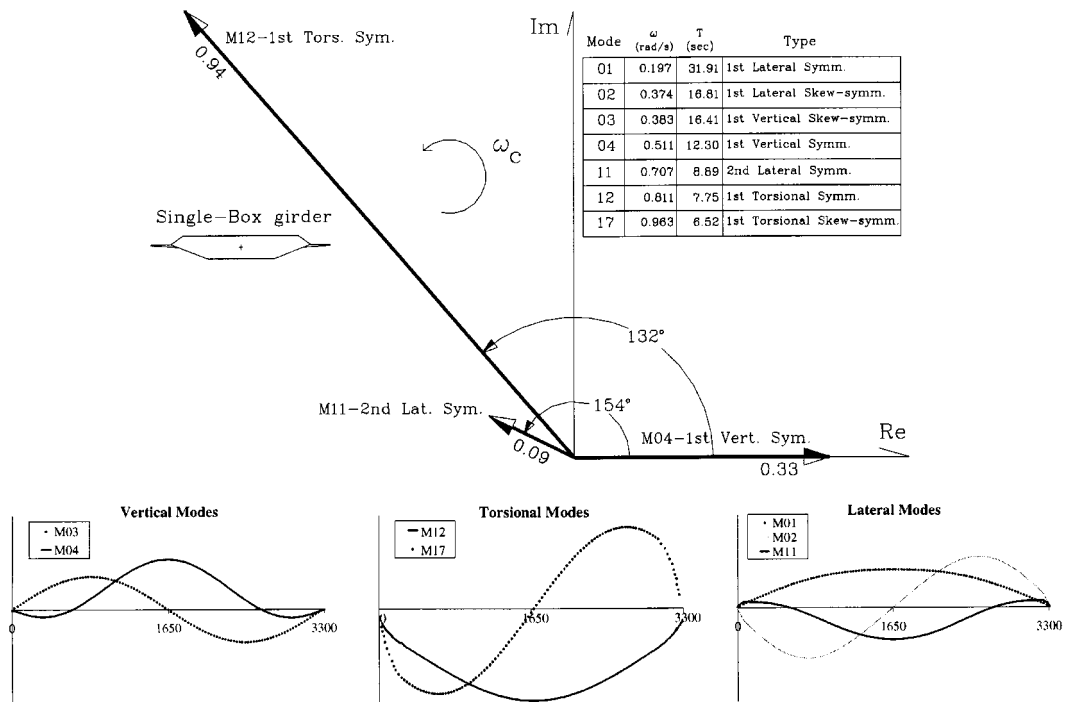


Fig. 9 Polar representation of the most significant contributions to the flutter mode for the example described in Sec. 3.1 (single-box “Humber-type” cross section)

In order to show the differences that may occur between the section model and the multimode method in the presence of very stiff decks, and since detailed data on the Akashi-Kaykio Bridge were not available, an example was built *ad hoc* starting from the original design of the Messina Bridge.

Namely, it was analysed a finite elements model with the same structural characteristics of the actual design, except for the deck, which has been substituted by a single-box girder with the same weight of the original one and with a cross-section similar to the Humber Bridge, and thus with the same aerodynamic characteristics (Fig. 8). In this case, while the first vertical and first torsional skew-symmetric modes (modes 3 and 17 in Fig. 9, respectively) are similar, the first couple of

symmetric modes (modes 4 and 12 in Fig. 9, respectively) have instead different shapes; in fact, while for the skew-symmetric modes and for the vertical symmetric one the shape is still dominated by the cable stiffness notwithstanding the increased stiffness of the girder deck, for the torsional symmetric mode the deck stiffness prevails on that of the cables.

As already said, the simplest formulation of the rigid section model (in writers' opinion the only one worth to be used for a preliminary assessment of the critical flutter speed) requires that the two modes considered (torsional and vertical) are perfectly similar; therefore for the example in this Section, this method can rigorously be applied only to the skew-symmetric modes 3 and 17, that turns a critical wind speed $U_c^{skew} = 62$ m/s.

On the contrary, the multimode analysis, performed by including both the above mentioned symmetric and skew-symmetric couples and the first three lateral modes, turns out a solution dominated by the symmetric modes (Fig. 9) and a lower critical wind speed $U_c^{mm} = 54$ m/s, with a difference that is small but certainly not negligible compared to U_c^{skew} .

Also by introducing in the section model the frequency and damping values corresponding to the first symmetric couple of modes (so pretending the perfect similarity among them) gives an error with the same order of magnitude, although on the safe side. In this case in fact the critical speed results $U_c^{sym} = 50$ m/s.

It can be observed from Fig. 9 that also in this example the contribution of lateral modes cannot be neglected.

4. Variations of time-average wind speed along the bridge axis

In previous sections the wind speed has been assumed as constant. However, as well known, the atmospheric turbulence and the consequent wind speed fluctuations can play a very significant role on the dynamic response.

Critical conditions of incipient aeroelastic instability are usually sought neglecting such fluctuations, that are considered as perturbations that can start auto-excited oscillations when mean wind speed is higher than the critical one; some of these aspects are taken into account by measuring aeroelastic derivatives in wind tunnel with a given intensity of turbulence of the approaching flow.

For very long span bridges, however, it can be appropriate to take into account a variation of time-average wind speed along the bridge axis, due for example to different topographic conditions. In such a case, denoting by \bar{U} a reference value of the wind speed (e.g., at mid-span) the time-average speed can be expressed as

$$U(x) = \bar{U} [1 + \psi(x)] \quad (8)$$

with an obvious meaning of $\psi(x)$; as a consequence, also aeroelastic forces are a function of x , and with the notation $\bar{K} = B\omega/\bar{U}$, they become (Eq. 3):

$$\begin{aligned} L_{se} &= \frac{1}{2} \rho \bar{U}^2 B \left[\bar{K} H_1^*(K) \frac{\dot{h}}{\bar{U}} + \bar{K} H_2^*(K) \frac{B \dot{\alpha}}{\bar{U}} + \bar{K}^2 H_3^*(K) \alpha \right] \\ D_{se} &= \frac{1}{2} \rho \bar{U}^2 B \left[\bar{K} P_1^*(K) \frac{\dot{p}}{\bar{U}} + \bar{K} P_2^*(K) \frac{B \dot{\alpha}}{\bar{U}} + \bar{K}^2 P_3^*(K) \alpha \right] \\ M_{se} &= \frac{1}{2} \rho \bar{U}^2 B^2 \left[\bar{K} A_1^*(K) \frac{\dot{h}}{\bar{U}} + \bar{K} A_2^*(K) \frac{B \dot{\alpha}}{\bar{U}} + \bar{K}^2 A_3^*(K) \alpha \right] \end{aligned} \quad (9)$$

Therefore, the forces corresponding to the reference wind speed \bar{U} and those corresponding to the

actual time average $U(x)$ variable along the x -axis differ from each other only because of the variation of aeroelastic derivatives with respect to their values $\bar{A}_i^*, \bar{H}_j^*, \bar{P}_k^*$ for $K=\bar{K}$.

The structure of Eqs. (A1) in Appendix is then unchanged, with the only difference that coefficients C_{jr}, D_{jr} of Eqs. (A2) have to be evaluated on the basis of the reference value \bar{U} , and integral coefficients $G(s_m, q_n)$ in Eq. (A3) should be re-defined as follows

$$G(s_m, q_n) = \int_{span} \lambda(x) s_m q_n dx ; s, q = h, p, \alpha ; m, n = 1, 2, \dots, N ; \quad (10)$$

$\lambda(x)$ in Eq. (10) denotes the ratio between the aeroelastic derivatives corresponding to $U(x)$ and to \bar{U} ; for example, the coefficient $G(\alpha_r, \alpha_j)$ appearing in the evaluation of C_{jr} (Eq. A2) becomes

$$G(\alpha_r, \alpha_j) = \int_{span} \lambda(x) \alpha_r \alpha_j dx, \quad \lambda(x) = \frac{A_3^*(x)}{\bar{A}_3^*} \quad (11)$$

Referring to the usual representation of aeroelastic derivatives as a function of the reduced velocity $v = 2\pi/K$ (cf. Sec. 5 and Fig. 4), and truncating the Taylor's series to the first order, $\lambda(x)$ in Eq. (11) becomes

$$\lambda(x) = \frac{A_3^*(v(x))}{\bar{A}_3^*} = \frac{1}{\bar{A}_3^*} \left[\bar{A}_3^* + \left(\frac{d}{dv} A_3^* \right)_{v=\bar{v}} (v(x) - \bar{v}) \right] = 1 + \Lambda \psi(x) \quad (12)$$

The constant Λ is the ratio between the slopes of the tangent to the curve $A_3^*(v)$ for $v = \bar{v} = 2\pi/\bar{K}$ and the slope of the secant to the same point, that is

$$\Lambda = \frac{\left(\frac{d}{dv} A_3^* \right)_{v=\bar{v}}}{\bar{A}_3^*/\bar{v}} \quad (13)$$

In an analogous way, defining the constant Λ on the basis of the appropriate aeroelastic derivative, it turns out in any case (Eqs. 10 and 12) that

$$G(s_m, q_n) = \int_{span} [1 + \Lambda \psi(x)] s_m q_n dx ; s, q = h, p, \alpha ; m, n = 1, 2, \dots, N \quad (14)$$

As a consequence, when modal shapes h_i, p_j, α_r are similar to each other (as those involved in the aerodynamic coupling leading to aeroelastic instability, cf. Sec. 2), only a variation $\psi(x)$ symmetric

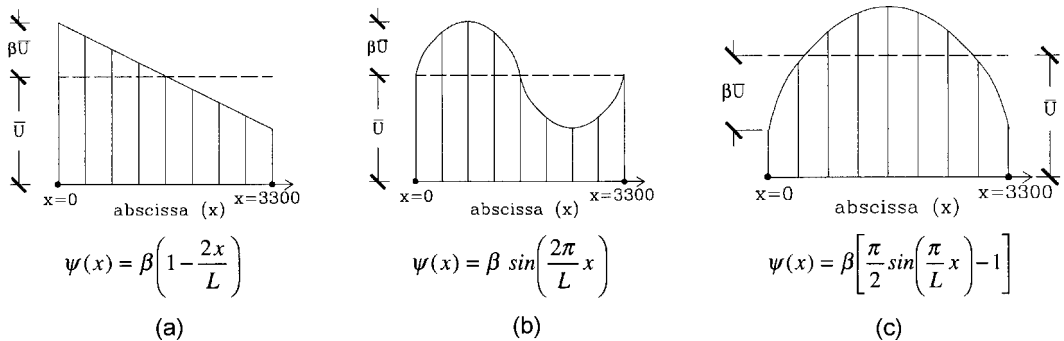


Fig. 10 Variation along the main span of the wind speed time-average

with respect to the bridge mid-span (Fig. 10c) (or at least with an average value different from zero) can affect coefficients $G(s_m, q_n)$ and therefore can have some influence on the stability conditions; on the opposite, skew-symmetric variations of the wind speed (Fig. 10a,b) cannot produce any effect, if they are so small that the first order approximation (Eq. 12) of the series expansion of aeroelastic derivatives can be accepted.

In any case, in the example under consideration the reduction of the critical wind speed amounts only to few meters per second, even if $\psi(x)$ is assumed as in Fig. 10c with a maximum wind speed variation of 10% with respect to the reference value \bar{U} .

5. Analysis in the time-domain

The values of flutter wind speed found in Sec. 3 and Sec. 4 are confirmed by numerical investigations performed in the time domain, using the same finite elements model of the bridge and increasing mean wind speeds until diverging oscillations are observed. The investigation has been conducted with a FORTRAN numerical code already implemented by one of the authors and tested for more than ten years, aimed to step-by-step analysis in the range of large displacements of nonlinear systems made up by linearly elastic one-dimensional finite elements, and improved with routines implemented *ad hoc* for wind-structure interaction.

The solution of the elastic problem is performed in terms of “total Lagrange’s coordinates”, taking into account system non-linearity through a discretization of the structure in a set of “cable-type” finite elements, with parabolic or rectilinear shape, while deck’s elements are “beam-type”. The associated system of equations (static problem) is solved by a second-order analysis, by means of an iterative procedure involving a succession of load steps, during which geometrical stiffness of the elements is continuously updated.

The dynamical analysis is performed through a step-by-step integration ($\Delta t = 0.2s$) of the motion equations, using the Newmark’s procedure. The mechanical damping has been assumed in accordance with Rayleigh’s method (coefficients $\alpha_R = 0.0015$ and $\beta_R = 0.0219$); the corresponding damping ratios ζ_j assume values between 0.6% and 0.8% for the principal modes responsible for aeroelastic instability (angular frequencies in the range 0.35-0.50 rad/s).

As concerns wind actions (drag, lift and moment), they have been concentrated on the deck, which has been divided in elements whose length is equal to the distance among hangers. The associated interaction forces depend on the instantaneous motion of the single section (Fig. 1).

Denoted by $f = \omega/(2\pi)$ the frequency of oscillation of the structure, the non-dimensional *reduced velocity* can be defined as

$$v = \frac{U}{Bf} = \frac{2\pi}{K} \quad (15)$$

and it turns to be equal to the ratio between the period of oscillation $T = 1/f$ and the time spent by the wind to cross the width B of the deck.

It is worth to observe that for very aerodynamic bridges, as the one under consideration, the reduced critical velocity is very high ($v_c > 20-30$); therefore, the oscillation corresponding to the flutter mode is so slow with respect to the time spent by the wind to cross the deck that, at each time, the aerodynamic forces can be defined by means of the static lift, drag and moment coefficients (Fig. 11), measured in wind tunnel (quasi-stationary approach, Zasso 1996).

Comparing the slopes of the curves in Fig. 11a,c it is evident that the already good behaviour

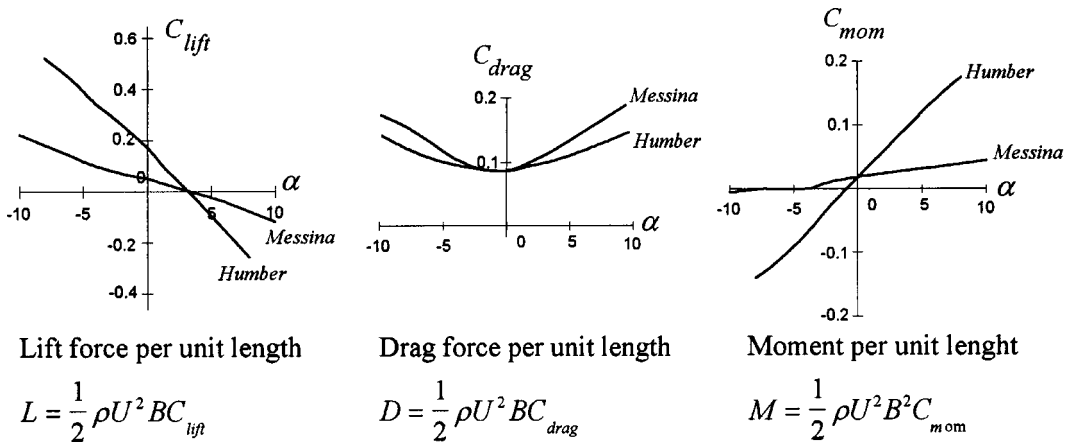


Fig. 11 Static coefficients of lift, drag and moment for the Humber and Messina bridges; α : angle of attack [deg]

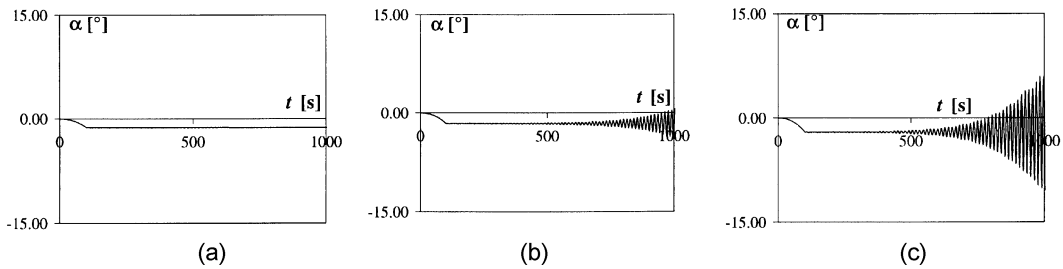


Fig. 12 Torsional rotation α [deg] of the cross section at a quarter of the main span; a) $U = 80$ m/s; b) $U = 90$ m/s; c) $U = 100$ m/s

found for the single-box deck of the Humber Bridge has been further improved for the three-box deck designed for the Messina Bridge.

Fig. 12 shows the rotation of a significant cross section of the bridge evaluated by time domain analyses, for wind speed equal to 80, 90 and 100 m/s, respectively, without turbulence. During the rising time of 100 seconds, when wind speed increases linearly from zero to its maximum value, the process can be considered as quasi-static; dynamic effects are found in the following part of the response for a wind speed U larger than approximately 90 m/s, and they correspond to self-excited oscillations with a period close to the one already found with the multimode analysis (about 15 seconds - Sec. 3).

The difference, very small indeed, between such critical value and those found in Sec. 3, can be attributed to the different characterisation of the aerodynamic forces (quasi-stationary approach in this section, aeroelastic derivatives in Sec. 3) and to the differences in their experimental evaluation.

6. Energetic approach

The multimodal approach discussed in previous sections allows to obtain a satisfactory and relatively simple evaluation of the critical wind speed for aeroelastic instability.

As shown, this critical value is also confirmed by numerical investigations in the time domain developed by means of a finite elements model.

Indeed, very detailed finite element models are often necessary and are in fact currently used also to evaluate the stress in the structural elements and the service-condition behaviour; such models give the response of the system to appropriate artificial wind time histories by means of step by step integration in the time domain, taking also into account non-linearities.

In this case, however, due to the large number of degrees of freedom (about 5000 in this example) it is often difficult to assess the critical wind speed on the base of displacement time histories of selected cross sections, *a priori* assumed as representative of the behaviour of the whole bridge.

It has deemed therefore interesting to discuss the results of the step by step numerical integration in terms of integral quantities, as the total energy of the structure at a given time or the work done by aerodynamic forces. As it will be shown in the following, in fact, the energy characterisation of the response gives an immediate clue to find not only the flutter wind speed, but also to evaluate the trend of divergence of critical oscillations and the contribution of the single components to the energy balance.

The direct evaluation of the energetic integral quantities is performed through the FORTRAN computer code described in Sec. 5, using routines and algorithms developed *ad hoc*. The different components of mechanical energy and the total work done by external aerodynamic loading are evaluated, and the energy dissipated by mechanical damping is found as the difference between the external work and the total energy.

The figures from 13 to 16 report the results of numerical simulations for three different values of the mean wind speed, $U_1 = 80$ m/s, $U_2 = 90$ m/s and $U_3 = 100$ m/s.

During the rising time interval (100 seconds), the total energy grows with an almost linear trend as a consequence of the work done by the “static” aerodynamic forces, that lead the structure from its initial equilibrium configuration to the deformed equilibrium configuration.

This is evident from Fig. 13, where the energy content at the end of the rising time interval is almost proportional to U^2 . This energy is mainly of the gravitational type, depending on the lateral displacement due to the quasi-static wind forces and on the consequent uplift of the deck. At this stage, in fact, lateral modes play a prominent role (e.g., *a* and *b* in Fig. 3), as it is confirmed by the “period” of the oscillation, of about 30 seconds.

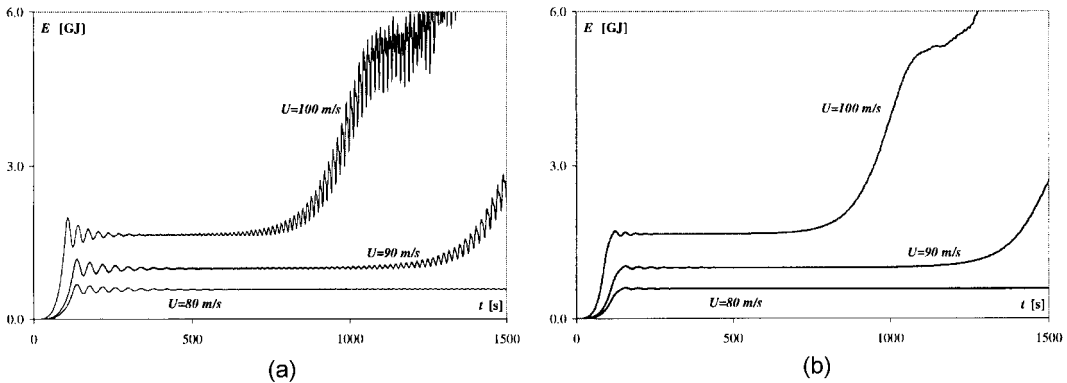


Fig. 13. Total energy E of the system (in $GJ = 10^9$ Joules) for wind speed $U = 80, 90$ and 100 m/s
a) time-history, b) moving averages on 40 seconds

In presence of a sufficiently high wind speed (more than about 90 m/s), a progressive and continuous transfer of energy from the fluid to the structure takes place, with a consequent amplification of structural oscillations. It is also evident (Fig. 13a) that these auto-excited oscillations have a shorter natural period (approximately equal to 15 seconds) with respect to those at the beginning of the loading process; in fact at this stage oscillations are prevalently due to the first pair of vertical and torsional modes, synchronised to a frequency comprised within the two natural frequencies as a consequence of the aerodynamic coupling.

In Fig. 13b it is shown the moving time-average of the total energy on a 40 seconds interval, that is sufficiently long to filter the fluctuations of the input energy during each oscillation period.

It is also evident from Fig. 13 that an accurate definition of the critical value of the wind speed cannot leave the duration of the time history out of consideration; in fact, a relatively smaller velocity applied for a longer period can produce larger effects than a higher velocity applied for a shorter time (1500 seconds at 90 m/s and 750 seconds at 100 m/s).

Fig. 14 shows the single components (moving averages on 40 seconds) of the total-energy for an oncoming flow with $U = 100$ m/s. It must be underlined that, although the wind action is only applied to the deck, the progressive growth of its oscillations induces a continuous energy transfer to the vertical towers and to the main suspension cables, where the greatest part of potential energy is concentrated (sum of the potential gravitational energy and the elastic deformation one).

It can be also observed that the elastic energy of the deck is much smaller with respect to that of the main cables, in the average less than 20%.

In a more recent release of the computer code, still being tested, it is also possible to consider wind action on the main cables, on the tower and on the hangers. Such effects, certainly relevant for the long span bridges recently built or designed, will be studied in the following part of this research.

Fig. 15 reports the comparison between the work done by aerodynamic forces and the total energy

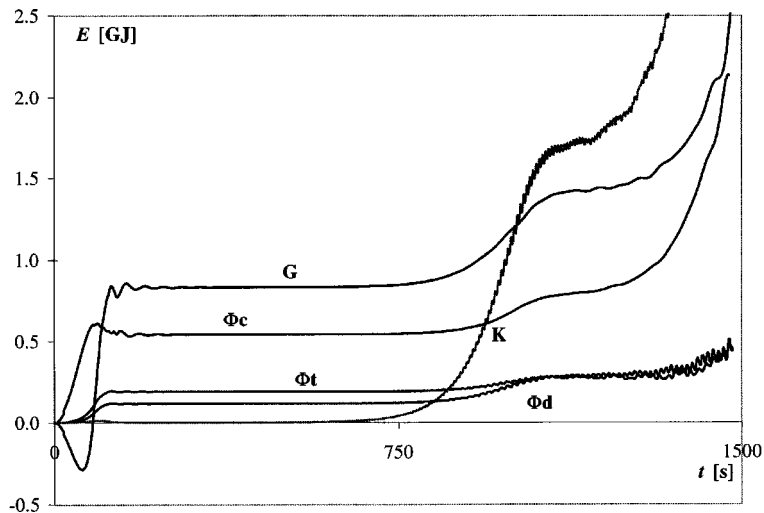


Fig. 14 Moving averages on 40 seconds of the components of the total energy E for wind speed $U = 100$ m/s: kinetic energy K , gravitational potential energy G and deformation energies Φ_c (cable elements), Φ_d (deck beams), Φ_t (towers)

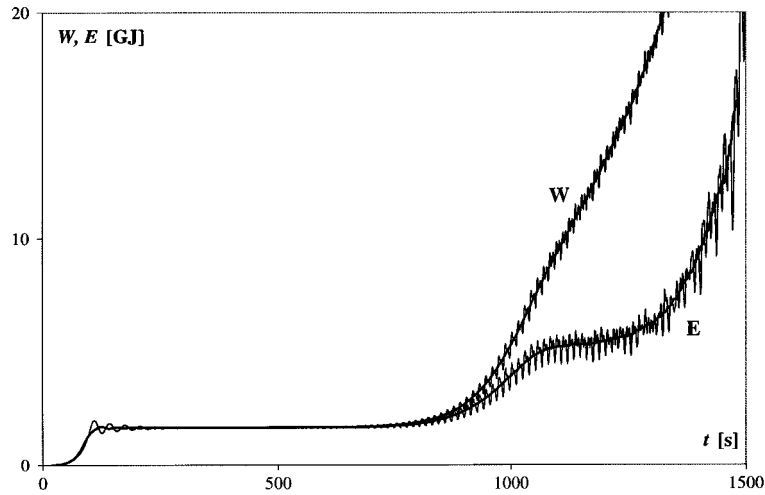


Fig. 15 Comparison between the work W done by the aerodynamic forces (*input energy*) and the total energy E . Time-history (thin line) and moving averages on 40 seconds (thick line). Mean wind speed $U = 100$ m/s

of the bridge for $U = 100$ m/s. It can be observed that in the last part of the time history both curves show diverging oscillations, corresponding to the passage from the quasi-static to the dynamic behaviour; the difference between the two functions represents the energy dissipated by the mechanical damping and it is more and more relevant for an increasing amplitude of the oscillations, reaching approximately the 25% of the aerodynamic work.

Finally, Fig. 16 shows the work done by each component of the aerodynamic interaction: lift, drag and moment. It is evident that during the wind speed rising interval, when the bridge displaces

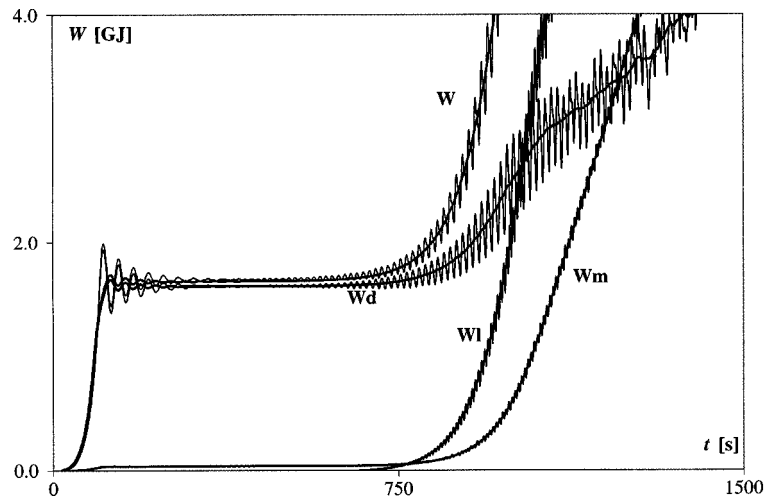


Fig. 16 Work W done by the aerodynamic forces and its components due to (Wl), drag (Wd) and moment (Wm). Time-history (thin line) and moving averages on 40 seconds (thick line). Mean wind speed $U = 100$ m/s

mainly in the lateral direction, only the drag forces make a significant work; at the opposite, also this representation of the response confirms that the aeroelastic instability can be mainly attributed to the work done by the aerodynamic forces during vertical and torsional displacements, although the contribution of the lateral component is not negligible.

7. Conclusions

The multimode approach to the aeroelastic instability of long-span suspension bridges is able to assess more accurately the critical wind speed and the shape of the *flutter mode* compared to the extremely simplified section model, with only a slightly larger computational cost. It has also been shown that this method can easily take into account phenomena that cannot be included within the section model, as the wind speed variability along the bridge's span. Further extensions of this method, currently under implementation, will allow to consider, with a limited increase of computational costs, the influence of semi-deterministic components of the turbulence and of the elastic local deformation of the deck cross section, an aspect that cannot be omitted for decks with an extremely complex behaviour, as the "multi-box" ones.

The paper describes also the convenience of representing the response in the time domain by means of integral measures, as the total energy of the system or the input energy, corresponding to the work done by forces due to fluid-structure interaction. This technique allows also to evaluate the beginning of the diverging oscillations related to aeroelastic instability more accurately than the usual representation of displacement components in the time-domain.

Acknowledgements

This work has been carried out in the framework of National Research Program "Researches and Experiments in Building Aerodynamics and Wind Engineering" (RESACIV), co-financed by the Italian "Ministry for University and Research" (MURST 1997-98). The "Stretto di Messina S.p.A." is also acknowledged for making available data and information on the design.

References

- D'Asdia, P. and Sepe, V. (1998), "Aeroelastic instability of long span suspended bridges: a multi-mode approach", *J. of Wind Eng. and Ind. Aerod.*, **74-76**, 849-857.
- Jain, A., Jones, N.P. and Scanlan, R.H. (1996), "Coupled aeroelastic and aerodynamic response analysis of long-span bridges", *J. of Wind Eng. and Ind. Aerod.*, **60**, 69-80.
- Katsuchi, H. (1997), "An analytical study on flutter and buffeting of the Akashi-Kaikyo Bridge", *MSc Thesis*, The Johns Hopkins University, Baltimore (USA).
- Katsuchi, H., Jones, N.P., Scanlan R.H. and Akiyama, H. (1997), "Multi-mode flutter and buffeting analysis of the Akashi-Kaikyo bridge", *Proceedings of 8th U.S. National Conference on Wind Engineering*, The Johns Hopkins University, Baltimore (USA), June.
- Scanlan, R.H. (1978), "The action of flexible bridges under wind, I: Flutter theory", *J. of Sound and Vibrations*, **60**(2), 187-199.
- Scanlan, R.H. (1987), "Interpreting aeroelastic models of cable-stayed bridges", *ASCE J. of Eng. Mech.*, **113**(4), 555-575.
- Scanlan, R.H. and Tomko, J.J. (1971), "Airfoil and bridge deck flutter derivatives", *ASCE J. of Eng. Mech.*, **97** (EM6), December, 1717-1737.
- Sepe, V., Ciappi, E. and D'Asdia, P. (1996), "Instabilità aeroelastica multimodale di ponti sospesi", *Proceedings*

of 4th Italian National Conferences on Wind Engineering (IN-VENTO-96), Trieste, September, 293-308, (in Italian).

Simiu, E. and Scanlan, R.H. (1996), *Wind Effects on Structures*, J. Wiley & Sons, 3rd Ed.

Tanaka, H., Yamamura, N. and Tatsumi, M. (1992), "Coupled mode flutter analysis using flutter derivatives," *J. of Wind Eng. and Ind. Aerod.*, **41/44**, 1279-1290.

Zasso, A. (1996), "Flutter derivatives: advantages of a new representation convention", *J. of Wind Eng. and Ind. Aerod.*, **60**, 35-47.

Appendix

Defining the generalised forces Q_j according to Eq. (3) and Eq. (4), the set of Eqs. (2) governing the dynamics can be derived in the frequency domain (Eq. 5), and in matrix form it reads

$$[C(K, \omega) + iD(K, \omega)]\xi_0 = 0 ; \quad (A1)$$

coefficients C_{jr} , D_{jr} of $N \times N$ matrices C , D are defined as follows

$$\begin{aligned} C_{jr} &= \delta_{jr}[-K^2 + K_j^2] - \frac{1}{2I_j} \rho B^4 K^2 [H_3^*(K)G(\alpha_r, h_j) + P_3^*(K)G(\alpha_r, p_j) + A_3^*(K)G(\alpha_r, \alpha_j)] \\ D_{jr} &= \delta_{jr} [2\zeta_j K_j K] - \frac{1}{2I_j} \rho B^4 K^2 \{ [H_1^*(K)G(h_r, h_j) + H_2^*(K)G(\alpha_r, h_j)] \\ &\quad + [P_1^*(K)G(p_r, p_j) + P_2^*(K)G(\alpha_r, p_j)] + [A_1^*(K)G(h_r, \alpha_j) + A_2^*(K)G(\alpha_r, \alpha_j)] \} \end{aligned} \quad (A2)$$

In Eq. (A2), δ_{jr} is the Kronecker symbol, $K_j = B\omega_j / U$ and $G(s_m, q_n)$ denotes the scalar product between the s and q components of the m -th and n -th natural modes, that is

$$G(s_m, q_n) = \int_{span} s_m q_n dx ; s, q = h, p, \alpha ; m, n = 1, 2, \dots, N \quad (A3)$$

The cross products $G(s_m, q_n)$ with $m \neq n$ correspond to the contribution given by displacements and velocities in the n -th mode to the m -th generalised force, and so they take into account the modal coupling due to aerodynamic forces.

(Communicated by Giovanni Solari)